Degenerate squeezing in a dual-pumped integrated microresonator: parasitic processes and their suppression

H. Seifoory,[1,2,*] Z. Vernon,[2] D. H. Mahler,[2] M. Menotti,[2] Y. Zhang,[2] and J. E. Sipe[1]

[1] *Department of Physics, University of Toronto, 60 St. George Street, Toronto, Ontario M5S 1A7, Canada*
[2] *Xanadu, Toronto, ON, M5G 2C8, Canada*

(Dated: September 9, 2021)

Using a general Hamiltonian treatment, we theoretically study the generation of degenerate quadrature squeezing in a dual-pumped integrated microring resonator coupled to a waveguide. Considering a dual-pump four-wave mixing configuration in an integrated Si_3N_4 platform, and following the coupled-mode theory approach, we investigate the effects of parasitic quantum nonlinear optical processes on the generation of squeezed light. Considering five resonance modes in this approach allows us to include the most important four-wave mixing processes involved in such a configuration. We theoretically explore the effects of the pump detunings on different nonlinear processes and show that the effects of some of the parasitic processes are effectively neutralized by symmetrically detuning the two pumps. This yields a significant enhancement in the output squeezing quality without physically changing the structure, but suffers from the trade-off of requiring substantially higher pump power for a fixed target level of squeezing.

arXiv:2109.03298v1 [quant-ph] 7 Sep 2021

I. INTRODUCTION

Squeezed states of light, in which the quantum fluctuations in one quadrature component are suppressed to a level below the quantum noise limit, have a wide range of applications in quantum metrology [1–4], quantum imaging [5–7], and communication [8, 9]. In addition, continuous variable (CV) entanglement can be efficiently produced using squeezed light and linear optics [10–12]. Of the methods used to generate squeezed states [13–16], the most common involve the use of either spontaneous four-wave mixing (SFWM) [17] or spontaneous parametric down conversion (SPDC) [18]. Implementations in bulk optics can suffer from scalability and complexity issues, but with the development of integrated photonics technology it is possible to overcome these limitations by integrating squeezed-light sources on one monolithic platform [19–22]. In particular, squeezed light generation via single-pass waveguides has been reported [23], and nonlinear optical resonators such as micro-ring resonators, whispering gallery mode resonators, and coupled-resonator optical waveguides can be employed to enhance the squeezing of the generated light [24–33].

Many CV protocols, such as CV quantum sampling[19], require squeezing in a single mode. One effective strategy for achieving this is based on dual-pump SFWM in microring resonators [19, 34]. In general, the SFWM process involves the conversion of two pump photons to signal and idler photons [35], where from energy conservation we have $\hbar\omega_{P_1} + \hbar\omega_{P_2} = \hbar\omega_S + \hbar\omega_I$, with ω_{P_1} and ω_{P_2} the two input frequencies, and ω_S and ω_I the generated signal and idler frequencies. For squeezing in a single mode, a prerequisite is to be in the degenerate squeezing regime, where the signal and idler frequencies are within the same resonance. However, other concurrent processes can lead to parasitic effects polluting the squeezed light [34, 36, 37]. The study of such parasitic processes is essential to the identification of proper suppression strategies.

In this work, we consider a ring resonator, made of a third-order nonlinear optical material such as silicon nitride (Si_3N_4), dual-pumped through a side-coupled waveguide. The optical properties of such a structure, schematically shown in Fig. 1a, can be studied theoretically using either the Lugiato-Lefever equations (LLE) or coupled mode theory (CMT). The former, which is a spatio-temporal method, requires the solution of only a single partial differential equation, and hence is computationally cost effective. However, it does not allow for an individual investigation of the consequences of each frequency mixing process. In contrast, for low enough input pump powers one can employ CMT, which is a spectro-temporal method, limited to only five resonances; we label them as $\{m, p_1, s, p_2, n\}$. As shown in Fig. 2, p_1 and p_2 are the two resonances used for pumping, s is the desired resonance for the squeezed light, and m and n are the adjacent resonances of p_1 and p_2, respectively. In this paper we use the CMT method to identify the role that the different frequency mixing processes play in determining the squeezing and anti-squeezing of light in resonance s, restricting ourselves to pump powers where an LLE analysis confirms that the restriction to five resonances is a reasonable approximation. This extends previous studies, where the calculations were limited to only three resonances, or only considered a single pump [26, 38]. The dual-pump configuration allows us to study degenerate squeezing, and the inclusion of the two adjacent resonances enables an investigation of the effects of parasitic processes on the squeezing.

The paper is organized as follows. In Secs. II-V we introduce the Hamiltonian terms associated with the ring fields, the channel fields, the coupling of the ring and channel, and the nonlinearity. With advances in both

* hossein.seifoory@utoronto.ca

the fabrication of integrated photonic structures and the measurement of their nonlinear quantum optical properties, a careful identification of the parameters that arise in the dynamical equations, which we present here, is in order. The correlation functions of interest are presented in Sec. VI, the dynamical equations that must be solved in Sec. VII, and the operator dynamics in Sec. VIII. The results for a sample structure are given in Sec. IX, and we conclude in Sec. X. Some of the calculation details are relegated to three appendices.

II. RING FIELDS

We begin by considering an isolated ring resonator as shown in Fig. 1a, but imagined far from any channel. A description that respects the symmetry uses the cylindrical coordinates z, the angle ϕ, and the radial coordinate $\rho = \sqrt{x^2+y^2}$; see Fig. 1. It is convenient to introduce a nominal radius R and use $\zeta = R\phi$ as a coordinate in place of ϕ. Denoting $\boldsymbol{r}_\perp = (\rho, z)$, a volume element is $d\boldsymbol{r} = d\boldsymbol{r}_\perp d\zeta$, where $d\boldsymbol{r}_\perp = R^{-1}\rho d\rho dz$, and ζ varies from 0 to $\mathcal{L} \equiv 2\pi R$. We assume that the linear response of the structure can be described by a relative dielectric constant $\varepsilon(\boldsymbol{r},\omega)$, and from the symmetry of the system the relative dielectric constant depends only on $\boldsymbol{r}_\perp$, $\varepsilon(\boldsymbol{r},\omega) = \varepsilon(\boldsymbol{r}_\perp,\omega)$. We label the modes of the ring by κ_J , the wave number associated with their propagation along the ring; we have $\kappa_J = 2\pi n_J/\mathcal{L}$, where n_j is an integer, and here we consider $n_J > 0$. We consider only one transverse field structure relevant for each κ_J, and identify its frequency by ω_J; this could be easily generalized. The Hamiltonian for the modes in the ring is then of the standard form,

$$H_{ring} = \sum_J \hbar\omega_J b_J^\dagger b_J, \tag{1}$$

neglecting the zero-point energy, as we do throughout; here

$$\left[b_J, b_{J'}^\dagger\right] = \delta_{JJ'} \tag{2}$$

as usual. It is convenient to specify the electromagnetic field amplitude of each mode in terms of the displacement field and magnetic field [26], in particular writing

$$\boldsymbol{D}(\boldsymbol{r}) = \sum_J \sqrt{\frac{\hbar\omega_J}{2}} b_J \boldsymbol{D}_J(\boldsymbol{r}) + H.c., \tag{3}$$

where

$$\boldsymbol{D}_J(\boldsymbol{r}) = \frac{\mathsf{d}_J(\boldsymbol{r}_\perp;\zeta)e^{i\kappa_J\zeta}}{\sqrt{\mathcal{L}}}. \tag{4}$$

The dependence of $\mathsf{d}_J(\boldsymbol{r}_\perp;\zeta)$ on ζ arises due to its components in the xy plane. As ζ varies they will lead to a change in direction of $\mathsf{d}_J(\boldsymbol{r}_\perp;\zeta)$, despite the fact that $\mathsf{d}_J^*(\boldsymbol{r}_\perp;\zeta)\cdot\mathsf{d}_J(\boldsymbol{r}_\perp;\zeta)$ will be independent of ζ; we can then take $\mathsf{d}_J^*(\boldsymbol{r}_\perp;\zeta)\cdot\mathsf{d}_J(\boldsymbol{r}_\perp;\zeta) = \mathsf{d}_J^*(\boldsymbol{r}_\perp;0)\cdot\mathsf{d}_J(\boldsymbol{r}_\perp;0)$. We can include dispersion effects in the normalization of each mode [39, 40] by taking

$$\int\int \frac{\mathsf{d}_J^*(\boldsymbol{r}_\perp;0)\cdot\mathsf{d}_J(\boldsymbol{r}_\perp;0)}{\epsilon_0\varepsilon(\boldsymbol{r}_\perp,\omega_J)}\frac{v_p(\boldsymbol{r}_\perp,\omega_J)}{v_g(\boldsymbol{r}_\perp,\omega_J)}d\boldsymbol{r}_\perp = 1. \tag{5}$$

where $v_p(\boldsymbol{r}_\perp,\omega_J)$ and $v_g(\boldsymbol{r}_\perp,\omega_J)$ are respectively the local phase and group velocities at the frequency ω_J of the mode; in general

$$v_p(\boldsymbol{r}_\perp,\omega) = c/n(\boldsymbol{r}_\perp,\omega), \tag{6}$$

$$v_g(\boldsymbol{r}_\perp,\omega) = v_p(\boldsymbol{r}_\perp,\omega)\left[1+\frac{\omega}{n(\boldsymbol{r}_\perp,\omega)}\frac{\partial n(\boldsymbol{r}_\perp,\omega)}{\partial\omega}\right]^{-1}, \tag{7}$$

where $n(\boldsymbol{r}_\perp,\omega) = \sqrt{\varepsilon(\boldsymbol{r}_\perp,\omega)}$ is the local index of refraction.

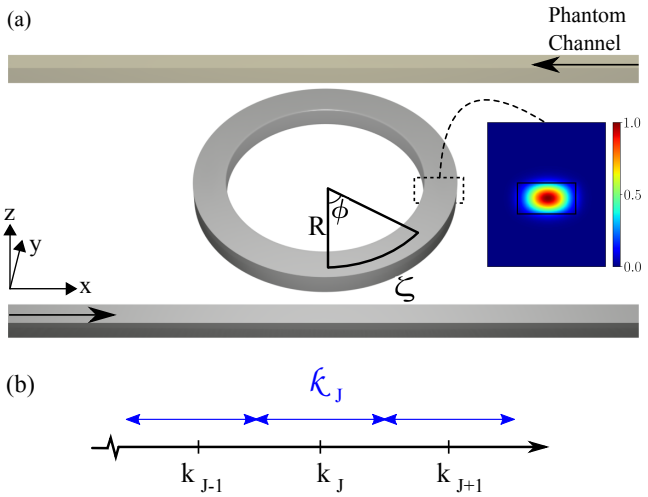


FIG. 1: (a) Schematic of microring resonator, with the nominal radius R, side-coupled to a physical channel and an effective phantom channel, which is introduced to account for scattering losses. The x coordinate for the phantom channel increases in the opposite direction to that of the real channel. The inset shows the electric field intensity of the fundamental mode at 1550 nm inside the ring. The parameters for the ring and channel are given in section X. (b) The range $\mathcal{K}_J$ of k, given by Eq. (11), associated with the J^{th} ring resonance

III. CHANNEL FIELDS

We next consider an isolated channel, as shown in the lower part of Fig. 1a, but imagined far from any ring. Here we take the channel to range along the x coordinate, and now use $\boldsymbol{r}_\perp = (y,z)$. Considering only one transverse field structure associated with each wave number k, in analogy with the treatment of the ring resonator, the

displacement field operator can be written [26]

$$\boldsymbol{D}(\boldsymbol{r}) = \int \sqrt{\frac{\hbar\omega_k}{4\pi}} a(k)\boldsymbol{d}_k(\boldsymbol{r}_\perp)e^{ikx}dk + H.c., \quad (8)$$

where ω_k is the frequency of the field characterized by k, the integral is over the range of k for which such modes exist, and

$$\left[a(k), a^\dagger(k')\right] = \delta(k-k'). \quad (9)$$

The $\boldsymbol{d}_k(\boldsymbol{r}_\perp)$ satisfy the normalization condition (5), with $\mathsf{d}_J(\boldsymbol{r}_\perp;0)$ replaced by $\boldsymbol{d}_k(\boldsymbol{r}_\perp)$ with $\boldsymbol{r}_\perp = (y,z)$. The Hamiltonian of the channel [26] is given by

$$H_{channel} = \int \hbar\omega_k a^\dagger(k)a(k)dk. \quad (10)$$

It is useful to break up the range of k in (8,10) into portions associated with each ring resonance. Letting k_J be the value of k for which $\omega_{k_J} = \omega_J$, the frequency of the J^{th} ring resonance, we set the range $\mathcal{K}_J$ of k associated with ring resonance J to be the values of k for which

$$k_J - \frac{(k_J - k_{J-1})}{2} < k \leq k_J + \frac{(k_{J+1} - k_J)}{2}, \quad (11)$$

(see Fig. 1b); then we write

$$\boldsymbol{D}(\boldsymbol{r}) = \sum_J \int_{\mathcal{K}_J} \sqrt{\frac{\hbar\omega_k}{4\pi}} a(k)\boldsymbol{d}_k(\boldsymbol{r}_\perp)e^{ikx}dk + H.c. \quad (12)$$
$$\approx \sum_J \sqrt{\frac{\hbar\omega_J}{2}} \boldsymbol{d}_J(\boldsymbol{r}_\perp)e^{ik_Jx}\psi_J(x) + H.c.,$$

where we have put $\boldsymbol{d}_J(\boldsymbol{r}_\perp) \equiv \boldsymbol{d}_{k_J}(\boldsymbol{r}_\perp)$ and

$$\psi_J(x) = \int_{\mathcal{K}_J} a(k)e^{i(k-k_J)x}\frac{dk}{\sqrt{2\pi}}. \quad (13)$$

In the second line of (12) we have neglected the variation of ω_k and $d_k(\boldsymbol{r}_\perp)$ as k varies over the range (11), and approximated them as ω_J and $\boldsymbol{d}_J(\boldsymbol{r}_\perp)$ respectively. Clearly $\psi_J(x)$ commutes with $\psi_{J'}(x')$ and $\psi^\dagger_{J'}(x')$ for $J' \neq J$; if the integral in (13) ranged from $-\infty$ to ∞ we would have

$$\left[\psi_J(x), \psi^\dagger_J(x')\right] = \delta(x-x'). \quad (14)$$

This is not exact, of course, but for fields $\psi_J(x)$ with relevant components k centered near k_J and far from the boundaries of $\mathcal{K}_J$ specified by (11) it will serve as a good approximation, and we adopt it. Breaking the integral in the Hamiltonian (10) into different resonance ranges $\mathcal{K}_J$, and neglecting group-velocity dispersion within each range by writing $\omega_k = \omega_J + v_J(k-k_J)$ in range $\mathcal{K}_J$, where v_J is the group velocity of the channel field at k_J, we have

$$H_{channel} = \sum_J \int_{\mathcal{K}_J} \hbar(\omega_J + v_J(k-k_J))a^\dagger(k)a(k)dk \quad (15)$$
$$= \sum_J \hbar\omega_J \int \psi^\dagger_J(x)\psi_J(x)dx$$
$$- \frac{1}{2}i\hbar\sum_J v_J \int \left(\psi^\dagger_J(x)\frac{\partial\psi_J(x)}{\partial x} - \frac{\partial\psi^\dagger_J(x)}{\partial x}\psi_J(x)\right)dx.$$

Finally, the operator for the total power flow in the waveguide is given by

$$P(x) = \int \boldsymbol{S}(\boldsymbol{r})\cdot\hat{\boldsymbol{x}}\; d\boldsymbol{r}_\perp, \quad (16)$$

where $\boldsymbol{S}(\boldsymbol{r})$ is the Poynting vector operator. Omitting terms that will be rapidly varying when we move to a Heisenberg picture, we find [41]

$$P(x) \to \sum_J \hbar\omega_J v_J \psi^\dagger_J(x)\psi_J(x). \quad (17)$$

IV. RING-CHANNEL COUPLING

We now adopt an effective point-coupling model between the channel and the ring (see Fig. 1a). If we take $\zeta = 0$ to correspond to the location on the ring closest to the channel, then the field in the ring at that point will include contributions from all the b_J with prefactors that will vary little as we move from one J to the next. Taking $x = 0$ to be the point in the channel closest to the ring, the Hamiltonian for an effective point-coupling model [26] is then

$$H_{coupling} = \sum_J \left(\hbar\gamma^*_J b^\dagger_J \psi(0) + H.c.\right), \quad (18)$$

where we expect the coupling constants γ_J to vary little as we move from one J to the next.

Most of the nonclassical attributes of light, such as squeezing and entanglement, are fragile with respect to loss [42–44]; this is an important issue when resonant structures are being studied. To take into account scattering losses in the ring we adopt a beam-splitter approach [26] by introducing a "phantom" channel (Fig. 1a) with a coupling to the ring given by

$$H^{ph}_{coupling} = \sum_J \left(\hbar\gamma^*_{Jph} b^\dagger_J \psi_{ph}(0) + H.c.\right), \quad (19)$$

where $\psi_{Jph}(x)$ is a field operator for the phantom channel,

$$\psi_{Jph}(x) = \int_{\mathcal{K}^{ph}_J} a_{ph}(k)e^{i(k-k_{Jph})x}\frac{dk}{\sqrt{2\pi}} \quad (20)$$

(cf. (13)), with a phantom channel Hamiltonian

$$H^{ph}_{channel} = \sum_J \int_{\mathcal{K}^{ph}_J} \hbar(\omega_J + v_{Jph}(k - k_{Jph})) \times a^\dagger_{ph}(k) a_{ph}(k) dk, \quad (21)$$

(cf. (15)), where γ_{Jph}, $a_{ph}(k)$, k_{Jph}, and v_{Jph} are the phantom channel analogs of the quantities γ_J, $a(k)$, k_J and v_J characterizing the actual channel and its coupling to the ring. We take the initial state of the phantom channel to be vacuum, and note that we take the x coordinate of the phantom channel to run in the opposite direction of that of the actual channel.

V. NONLINEARITY

For the $\chi^{ijkl}_{(3)}$ nonlinearity considered here, the nonlinear Hamiltonian is given [39, 45, 46] by

$$H_{NL} = -\frac{1}{4\epsilon_0} \int d\boldsymbol{r} \Gamma^{ijkl}_{(3)}(\boldsymbol{r}) D^i(\boldsymbol{r}) D^j(\boldsymbol{r}) D^k(\boldsymbol{r}) D^l(\boldsymbol{r}), \quad (22)$$

where neglecting dispersion in this term we have

$$\Gamma^{ijkl}_{(3)}(\boldsymbol{r}) = \frac{\chi^{ijkl}_{(3)}(\boldsymbol{r})}{\epsilon_0^2 n^8(\boldsymbol{r})}, \quad (23)$$

with $n(\boldsymbol{r})$ is the local index of refraction; we take the integral in (22) to range over the volume of the ring, where the nonlinear effect will be important. In this paper we focus on five resonances of interest, taking the index J in equations such as (3) to range over the labels $\{m, p_1, s, p_2, n\}$ (see Fig. 2). Here p_1 and p_2 label the two strong pumps, leading to the generation of photons within resonances m, s, and n by nonlinear processes we detail below; since the frequencies of these five resonances are very close, the neglect of dispersion in (23) should be a good approximation. Using the displacement field (3) in (22), and neglecting corrections due to normal ordering, we find

$$H_{NL} = -\frac{\hbar}{2} \sum_{J,K,L,M} \Lambda_{JKLM} b^\dagger_J b^\dagger_K b_L b_M, \quad (24)$$

where we have kept only the terms involving two creation and annihilation operators, since the others will be rapidly varying in an interaction picture and can be neglected, and

$$\Lambda_{JKLM} = \frac{3\hbar}{4\epsilon_0} \sqrt{\omega_J \omega_K \omega_L \omega_M} \times \int d\boldsymbol{r} \Gamma^{ijkl}_{(3)}(\boldsymbol{r}) \left(D^i_J(\boldsymbol{r}) D^j_K(\boldsymbol{r}) \right)^* D^k_L(\boldsymbol{r}) D^l_M(\boldsymbol{r}). \quad (25)$$

where we have used (3), and $\Delta\kappa = \kappa_L + \kappa_M - \kappa_J - \kappa_K = 0$ for the energy conserving terms. Again, since the frequencies of the five resonances of interest are close to each other, and thus to a reference frequency ω, for the energy conserving terms that arise all the coefficients of Λ_{JKLM} are essentially the same, and we can set $\Lambda_{JKLM} \to \Lambda$. In Appendix A we show that

$$\Lambda = \frac{\hbar \omega v^2 \gamma}{\mathcal{L}}, \quad (26)$$

where v is the group velocity of light propagating in the ring, and γ is the waveguide nonlinear parameter. This corrects a factor of two error that appeared in a recent study [19], and is in agreement with earlier work [47].

The relevant processes described by H_{NL}, and their associated Hamiltonians, are then self-phase modulation (SPM),

$$H_{SPM} = -\hbar \frac{\Lambda}{2} \left(b^\dagger_{p_1} b^\dagger_{p_1} b_{p_1} b_{p_1} + b^\dagger_{p_2} b^\dagger_{p_2} b_{p_2} b_{p_2} \right), \quad (27)$$

and cross-phase modulation (XPM),

$$H_{XPM} = -2\hbar\Lambda \left(b^\dagger_s b^\dagger_{p_1} b_s b_{p_1} + b^\dagger_s b^\dagger_{p_2} b_s b_{p_2} + b^\dagger_{p_1} b^\dagger_{p_2} b_{p_1} b_{p_2} + b^\dagger_m b^\dagger_{p_1} b_m b_{p_1} + b^\dagger_m b^\dagger_{p_2} b_m b_{p_2} + b^\dagger_n b^\dagger_{p_1} b_n b_{p_1} + b^\dagger_n b^\dagger_{p_2} b_n b_{p_2} \right), \quad (28)$$

which lead to frequency shifts of the ring resonances, together with dual-pump spontaneous four-wave mixing (DP-SFWM),

$$H_{DP-SFWM} = -\hbar\Lambda b^\dagger_s b^\dagger_s b_{p1} b_{p2} + H.c., \quad (29)$$

single-pump SFWM (SP-SFWM),

$$H_{SP-SFWM} = -\hbar\Lambda \left(b^\dagger_m b^\dagger_s b_{p_1} b_{p_1} + b^\dagger_n b^\dagger_s b_{p_2} b_{p_2} \right) + H.c., \quad (30)$$

Bragg-scattering FWM (BS-FWM),

$$H_{BS-FWM} = -2\hbar\Lambda \left(b^\dagger_{p_2} b^\dagger_m b_{p_1} b_s + b^\dagger_{p_1} b^\dagger_n b_{p_2} b_s \right) + H.c., \quad (31)$$

and hyper-parametric SFWM,

$$H_{HP-SFWM} = -2\hbar\Lambda b^\dagger_m b^\dagger_n b_{p1} b_{p2} + H.c., \quad (32)$$

which are processes that lead to transitions between the different resonances. These processes, and the associated resonances involved, are illustrated in Fig. 2. For each process the solid lines indicate the transitions that will be more important for the excitation scenario considered; the dotted lines, corresponding to the Hamiltonian terms denoted by $+H.c.$ in the expressions above, indicate the reverse transitions. For example, for DP-SFWM, which is the desired process for producing degenerate squeezed vacuum states in resonance s, the important transitions are those where pump photons from p_1 and p_2 are destroyed and two photons in resonance s are created; the reverse transition, where two photons from resonance s are destroyed and pump photons at p_1 and p_2 are created, will be less important since there will always be many more photons in p_1 and in p_2 than in s.

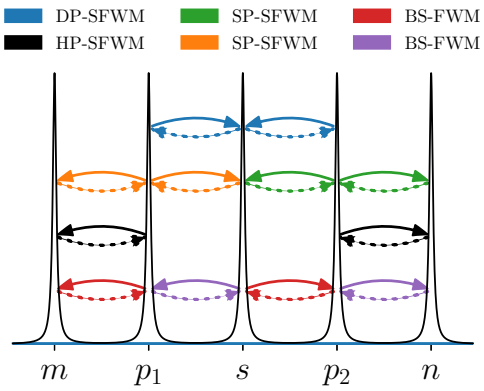


FIG. 2: (Color online) Four-wave mixing processes that occur in a ring resonator when two resonances p_1 and p_2 are pumped. DP-SFWM leads to squeezing of the s mode while the unwanted processes of SP-SFWM and BS-FWM generate noise and impurify the output. The corresponding conjugate of each process is shown with the dotted arrows with the same color.

Finally, then, we can then write

$$H_{NL}\left(\{b_K\},\left\{b_L^\dagger\right\}\right) = H_{DP-SFWM} + H_{SPM} + H_{XPM} + H_{SP-SFWM} + H_{BS-FWM} + H_{HP-SFWM}. \quad (33)$$

VI. CORRELATION FUNCTIONS

We now write our full Hamiltonian as

$$H = H_0 + V(\{\mathcal{A}_i\}), \quad (34)$$

where

$$H_0 = H_{ring} + H_{channel} + H^{ph}_{channel}, \quad (35)$$
$$V(\{\mathcal{A}_i\}) = H_{coupling} + H^{ph}_{coupling} + H_{NL}\left(\{b_J\},\left\{b_L^\dagger\right\}\right),$$

and the set $\{\mathcal{A}_i\}$ consists of all the Schrödinger operators appearing in $H_{coupling}$, $H^{ph}_{coupling}$, and $H_{NL}\left(\{b_J\},\left\{b_L^\dagger\right\}\right)$. The evolution operators $\mathcal{U}_0(t,t')$ and $\mathcal{U}(t,t')$ for H_0 and $H(t)$, respectively, satisfy

$$i\hbar\frac{\partial}{\partial t}\mathcal{U}_0(t,t') = H_0\mathcal{U}_0(t,t'), \quad (36)$$
$$i\hbar\frac{\partial}{\partial t}\mathcal{U}(t,t') = H(t)\mathcal{U}(t,t'), \quad (37)$$

with $\mathcal{U}(t,t) = \mathcal{U}_0(t,t) = \mathbb{I}$ for all t.

For the Hamiltonians H and the initial kets we consider, there will be times t_{min} and t_{max} such that for all times $t < t_{min}$ and all times $t > t_{max}$ the term $V(\{\mathcal{A}_i\})$ will have no effect on the evolution of the Schrödinger ket $|\Psi(t)\rangle$. We choose $t_0 < t_{min}$ and $t_1 > t_{max}$, and define

$$|\Psi_{in}\rangle = \mathcal{U}_0(0,t_0)\,|\Psi(t_0)\rangle\,, \quad (38)$$
$$|\Psi_{out}\rangle = \mathcal{U}_0(0,t_1)\,|\Psi(t_1)\rangle\,. \quad (39)$$

Then, since $|\Psi(t_1)\rangle = \mathcal{U}(t_1,t_0)\,|\Psi(t_0)\rangle$ we have

$$|\Psi_{out}\rangle = U(t_1,t_0)\,|\Psi_{in}\rangle = U(\infty,-\infty)\,|\Psi_{in}\rangle\,, \quad (40)$$

where

$$U(t,t') \equiv \mathcal{U}_0(0,t)\mathcal{U}(t,t')\mathcal{U}_0(t',0), \quad (41)$$

and the extension to $\pm\infty$ in the second line of (40) follows because in the added times $V(\{\mathcal{A}_i\})$ has no effect. This is the approach of scattering theory. For our applications in this paper we will be primarily interested in correlation functions, and so a Heisenberg strategy, which is however connected to this, will be more useful.

Defining Heisenberg operators referenced to t_0 in the usual way,

$$\mathcal{A}_i^H(t) = \mathcal{U}^\dagger(t,t_0)\mathcal{A}_i\mathcal{U}(t,t_0), \quad (42)$$

we use (41) to write $\mathcal{U}(t,t_0)$ in terms of $U(t,t_0)$ and $\mathcal{U}_0$, and we find

$$\mathcal{A}_k^H(t) = \mathcal{U}_0^\dagger(0,t_0)\left(\sum_l g_{kl}(t)\bar{\mathcal{A}}_l(t)\right)\mathcal{U}_0(0,t_0). \quad (43)$$

Here

$$\bar{\mathcal{A}}_l(t) = U^\dagger(t,-\infty)\mathcal{A}_l U(t,-\infty), \quad (44)$$

where we have used the fact that $U(t,t_0) = U(t,-\infty)$, while the $g_{kl}(t)$ are the functions that characterize an evolution according to only H_0,

$$\mathcal{U}_0^\dagger(t,0)\mathcal{A}_i\mathcal{U}_0(t,0) = \sum_j g_{ij}(t)\mathcal{A}_j. \quad (45)$$

and we have taken the set $\{\mathcal{A}_i\}$ to be expanded, if necessary, so that these equations can be written for the $\mathcal{A}_i$ originally appearing in $V(\{\mathcal{A}_i\};t)$; we will see examples of (45), and its extensions, below. The $\bar{\mathcal{A}}_l(t)$ are easily seen to satisfy the equations

$$i\hbar\frac{d}{dt}\bar{\mathcal{A}}_l(t) = \left[\bar{\mathcal{A}}_l(t), V\left(\left\{\sum_j g_{ij}(t)\bar{A}_j(t)\right\}\right)\right], \quad (46)$$

with the initial conditions $\bar{\mathcal{A}}_l(-\infty) = \mathcal{A}_l$. Using (43) we then have

$$\langle\Psi(t)|\mathcal{A}_k|\Psi(t)\rangle = \langle\Psi(t_0)|\mathcal{A}_k^H(t)|\Psi(t_0)\rangle = \sum_l g_{kl}(t)\,\langle\Psi_{in}|\bar{\mathcal{A}}_l(t)|\Psi_{in}\rangle\,, \quad (47)$$

$$\left\langle \Psi(t_0)|\mathcal{A}_k^H(t)\mathcal{A}_l^H(t')|\Psi(t_0)\right\rangle = \sum_{l,j} g_{kl}(t)g_{ij}(t')\left\langle \Psi_{in})|\bar{\mathcal{A}}_l(t)\bar{\mathcal{A}}_j(t')|\Psi_{in}\right\rangle, \quad (48)$$

and so on for higher order correlation functions, for arbitrary times t and t'. Since for $t > t_{max}$ we have $U(t,-\infty) = U(\infty,-\infty)$, if t and t' are greater than t_{max} we have

$$\left\langle \Psi(t_0)|\mathcal{A}_k^H(t)|\Psi(t_0)\right\rangle \to \sum_l g_{kl}(t)\left\langle \Psi_{in}|\bar{\mathcal{A}}_l(\infty)|\Psi_{in}\right\rangle, \quad (49)$$

$$\left\langle \Psi(t_0)|\mathcal{A}_k^H(t)\mathcal{A}_l^H(t')|\Psi(t_0)\right\rangle \to \sum_{l,j} g_{kl}(t)g_{ij}(t')\left\langle \Psi_{in})|\bar{\mathcal{A}}_l(\infty)\bar{\mathcal{A}}_j(\infty)|\Psi_{in}\right\rangle, \quad (50)$$

and the remaining dynamics, governed only by H_0 is captured by the $g_{ij}(t)$.

VII. DYNAMICAL EQUATIONS

In Appendix B we show that

$$\begin{aligned} &V\left(\left\{\sum_j g_{ij}(t)\bar{\mathcal{A}}_j(t)\right\}\right) \quad (51)\\ &= \hbar\sum_J \gamma_J^*\bar{b}_J(t)\bar{\psi}_J(-v_Jt,t) + H.c.\\ &+ \hbar\sum_J \gamma_{Jph}^*\bar{b}_J(t)\bar{\psi}_{Jph}(-v_{Jph}t,t) + H.c.\\ &+ H_{NL}\left(\left\{\bar{b}_K(t)e^{-i\omega_K t}\right\},\left\{\bar{b}_L^\dagger(t)e^{i\omega_L t}\right\}\right), \end{aligned}$$

where, for example, $\bar{\psi}(-v_Jt,t)$, is the operator $\bar{\psi}(x,t)$ (see (44)) evaluated at $x = -v_Jt$. Using this in (46) we find the equation for $\bar{\psi}_J(x,t)$ is

$$i\hbar\frac{\partial\bar{\psi}_J(x,t)}{\partial t} = \hbar\gamma_J\bar{b}_J(t)\delta(x+v_Jt), \quad (52)$$

and subject to the initial condition $\bar{\psi}_J(x,-\infty) = \psi_J(x)$ the solution is

$$\bar{\psi}_J(x,t) = \psi_J(x) - i\frac{\gamma_J}{v_J}\bar{b}_J\left(-\frac{x}{v_J}\right)\theta(t+\frac{x}{v_J}), \quad (53)$$

where as usual $\theta(t) = 1, 1/2, 0$ as $t > 0, = 0, < 0$; thus

$$\bar{\psi}_J(-v_Jt,t) = \psi_J(-v_Jt) - i\frac{\gamma_J}{2v_J}\bar{b}_J(t), \quad (54)$$

and similarly for $\bar{\psi}_{Jph}(-v_{Jph}t,t)$. Using these results in the equation (46) for $\bar{b}_J(t)$ we find

$$\begin{aligned} &\left(\frac{d}{dt}+\bar{\Gamma}_J\right)\bar{b}_J(t) = s_J(t)\\ &+ \frac{1}{i\hbar}\left[\bar{b}_J(t), H_{NL}\left(\left\{\bar{b}_K(t)e^{-i\omega_K t}\right\},\left\{\bar{b}_L^\dagger(t)e^{i\omega_L t}\right\}\right)\right], \end{aligned} \quad (55)$$

where the Schrödinger operator

$$s_J(t) = -i\gamma_J^*\psi_J(-v_Jt) - i\gamma_{Jph}^*\psi_{Jph}(-v_{Jph}t), \quad (56)$$

and

$$\bar{\Gamma}_J \equiv \frac{|\gamma_J|^2}{2v_J} + \frac{|\gamma_{Jph}|^2}{2v_{Jph}} \quad (57)$$

describes the decay of the field in the ring due to coupling to the channel and the scattering losses, the latter described by coupling to the phantom channel.

VIII. OPERATOR DYNAMICS

For the resonances $L = p_1, p_2$ associated with the two pumps we make the classical approximation, taking $\psi_L(-v_Lt) \to \langle\psi_L(-v_Lt)\rangle$, where in the center of long incident pump pulses we put

$$\langle\psi_L(-v_Lt)\rangle = \sqrt{\frac{P_L}{v_L\hbar\omega_L}}e^{-i\Delta_Lt} \equiv C_Le^{-i\Delta_Lt} \quad (58)$$

(cf. (17)), defining a CW approximation; here P_L is the incident power, and Δ_L a detuning from the ring resonance at ω_L. Similarly, for $L = p_1, p_2$ we take $\bar{b}_L(t) \to \langle\bar{b}_L(t)\rangle \equiv \beta_L(t)$. Then the classical limit of the equations (55) can be constructed for $\beta_{p_1}(t)$ and $\beta_{p_2}(t)$, and introducing

$$F_{p_1}(t) \equiv \beta_{p_1}(t)\,e^{i\Delta_{p_1}t}, \quad (59)$$

$$F_{p_2}(t) \equiv \beta_{p_2}(t)\,e^{i\Delta_{p_2}t}, \quad (60)$$

they can be written as

$$\begin{aligned} &\left(\frac{d}{dt}+\bar{\Gamma}_{p_1} - i\Lambda\left(|F_{p_1}(t)|^2 + 2|F_{p_2}(t)|^2\right) - i\Delta_{p_1}\right)F_{p_1}(t)\\ &= -i\gamma_{p_1}^*C_{p_1}, \end{aligned} \quad (61)$$

$$\begin{aligned} &\left(\frac{d}{dt}+\bar{\Gamma}_{p_2} - i\Lambda\left(|F_{p_2}(t)|^2 + 2|F_{p_1}(t)|^2\right) - i\Delta_{p_2}\right)F_{p_2}(t)\\ &= -i\gamma_{p_2}^*C_{p_2}, \end{aligned} \quad (62)$$

in which we have assumed there is no incoming pump energy in the phantom channel. The steady state solutions of these equations are affected by SPM and XPM, which determine the resonant frequencies of the structure in the presence of the nonlinearity. We refer to these new resonant frequencies as the "hot-cavity resonances." Note that these two equations can easily be solved numerically for the steady-state values of F_{p_1} and F_{p_2}, and one can use the transformations (59) and (60) to determine the quantities $\beta_{p_1}(t)$ and $\beta_{p_2}(t)$.

With these in hand we can construct the equations for the fluctuating quantities,

$$\tilde{b}_J(t) \equiv \bar{b}_J(t) - \left\langle\bar{b}_J(t)\right\rangle, \quad (63)$$

which will be driven by the quantities

$$\tilde{s}_J(t) \equiv \bar{d}_J(t) - \left\langle \bar{d}_J(t) \right\rangle, \tag{64}$$

where since $\langle \bar{s}_J(t) \rangle = 0$ for $J = m, s, n$ we have $\left\langle \bar{b}_J(t) \right\rangle = 0$ for those J. For reasons we discuss below, it is convenient to work with the quantities

$$f_J(t) \equiv \tilde{b}_J(t)\, e^{iR_J t}, \tag{65}$$

where

$$R_s = \frac{\Delta_{p_1} + \Delta_{p_2}}{2} + \frac{\omega_{p_1} + \omega_{p_2} - 2\omega_s}{2}, \tag{66}$$

$$R_{p_1} = \Delta_{p_1}, \tag{67}$$

$$R_{p_2} = \Delta_{p_2}, \tag{68}$$

$$R_m = \frac{3\Delta_{p_1} - \Delta_{p_2}}{2} + \frac{3\omega_{p_1} - \omega_{p_2} - 2\omega_m}{2}, \tag{69}$$

$$R_n = \frac{3\Delta_{p_2} - \Delta_{p_1}}{2} + \frac{3\omega_{p_2} - \omega_{p_1} - 2\omega_n}{2}. \tag{70}$$

These are detuning-like quantities; in the limit where group-velocity dispersion is negligible and both pumps are equally detuned, $\Delta_{p_2} = \Delta_{p_1} = \Delta$, all the R parameters are equal to that single detuning, $R_J = \Delta$.

The resulting dynamical equations,

$$\begin{aligned}
&\left(\frac{d}{dt} + \bar{\Gamma}_s - iR_s\right) f_s(t) = \tilde{s}_s(t)\, e^{iR_s t} \\
&+ 2i\Lambda \left(F_{p_1}(t)\, F_{p_2}(t)\, f_s^\dagger(t) + F_{p_1}^*(t)\, F_{p_2}(t)\, f_m(t)\right. \\
&+ F_{p_2}^*(t)\, F_{p_1}(t)\, f_n(t) + F_{p_1}^*(t)\, F_{p_1}(t)\, f_s(t) \\
&\left. + F_{p_2}^*(t)\, F_{p_2}(t)\, f_s(t)\right) \\
&+ i\Lambda \left(F_{p_1}(t)\, F_{p_1}(t)\, f_m^\dagger(t) + F_{p_2}(t)\, F_{p_2}(t)\, f_n^\dagger(t)\right),
\end{aligned} \tag{71}$$

$$\begin{aligned}
&\left(\frac{d}{dt} + \bar{\Gamma}_m - iR_m\right) f_m(t) = \tilde{s}_m(t)\, e^{iR_m t} \\
&+ 2i\Lambda \left(F_{p_2}^*(t)\, F_{p_1}(t)\, f_s(t) + F_{p_1}^*(t)\, F_{p_1}(t)\, f_m(t)\right. \\
&\left. + F_{p_2}^*(t)\, F_{p_2}(t)\, f_n(t)\right) \\
&+ i\Lambda \left(2F_{p_1}(t)\, F_{p_2}(t)\, f_n^\dagger(t) + F_{p_1}(t)\, F_{p_1}(t)\, f_s^\dagger(t)\right),
\end{aligned} \tag{72}$$

$$\begin{aligned}
&\left(\frac{d}{dt} + \bar{\Gamma}_n - iR_n\right) f_n(t) = \tilde{s}_n(t)\, e^{iR_n t} \\
&+ 2i\Lambda \left(F_{p_1}^*(t)\, F_{p_2}(t)\, f_s(t) + F_{p_1}^*(t)\, F_{p_1}(t)\, f_n(t)\right. \\
&\left. + F_{p_2}^*(t)\, F_{p_2}(t)\, f_n(t)\right) \\
&+ i\Lambda \left(2F_{p_1}(t)\, F_{p_2}(t)\, f_m^\dagger(t) + F_{p_2}(t)\, F_{p_2}(t)\, f_s^\dagger(t)\right),
\end{aligned} \tag{73}$$

$$\begin{aligned}
&\left(\frac{d}{dt} + \bar{\Gamma}_{p_1} - iR_{p_1}\right) f_{p_1}(t) = \tilde{s}_{p_1}(t)\, e^{iR_{p_1} t} \\
&+ 2i\Lambda \left(|F_{p_2}(t)|^2 + |F_{p_1}(t)|^2\right) f_{p_1}(t) \\
&+ 2i\Lambda\, F_{p_2}^*(t)\, F_{p_1}(t)\, f_{p_2}(t) + 2i\Lambda\, F_{p_1}(t)\, F_{p_2}(t)\, f_{p_2}^\dagger(t) \\
&+ i\Lambda\, F_{p_1}^2(t)\, f_{p_1}^\dagger(t),
\end{aligned} \tag{74}$$

$$\begin{aligned}
&\left(\frac{d}{dt} + \bar{\Gamma}_{p_2} - iR_{p_2}\right) f_{p_2}(t) = \tilde{s}_{p_2}(t)\, e^{iR_{p_2} t} \\
&+ 2i\Lambda \left(|F_{p_2}(t)|^2 + |F_{p_1}(t)|^2\right) f_{p_2}(t) \\
&+ 2i\Lambda\, F_{p_1}^*(t)\, F_{p_2}(t)\, f_{p_1}(t) + 2i\Lambda\, F_{p_2}(t)\, F_{p_1}(t)\, f_{p_1}^\dagger(t) \\
&+ i\Lambda\, F_{p_2}^2(t)\, f_{p_2}^\dagger(t),
\end{aligned} \tag{75}$$

can be written in matrix form,

$$\frac{d}{dt}\mathcal{F}(t) = \mathbb{M}(t)\ \mathcal{F}(t) + \mathcal{D}(t), \tag{76}$$

where

$$\mathcal{F}(t) = \begin{pmatrix} \uparrow \\ f_l(t) \\ \downarrow \\ \uparrow \\ f_l^\dagger(t) \\ \downarrow \end{pmatrix}, \tag{77}$$

$$\mathcal{D}(t) = \begin{pmatrix} \uparrow \\ \tilde{s}_l(t)\, e^{iR_l t} \\ \downarrow \\ \uparrow \\ \tilde{s}_l^\dagger(t)\, e^{-iR_l t} \\ \downarrow \end{pmatrix}, \tag{78}$$

and $\mathbb{M}(t)$ is a matrix, the components of which can be read from (71,72,73,74,75). From the form (76) we can construct a formal solution by introducing a Green matrix $\mathbb{G}(t, t')$ satisfying

$$\frac{d\mathbb{G}(t, t')}{d\tau} = \mathbb{M}(t)\ \mathbb{G}(t, t'), \tag{79}$$

and $\mathbb{G}(t', t') = \mathbb{I}$ for all t'. We find the solution of (76) as

$$\mathcal{F}(t) = \mathbb{G}(t, t_0)\ \mathcal{F}(t_0) + \int_{t_0}^{t} \mathbb{G}(t, t')\ \mathcal{D}(t')\ dt'. \tag{80}$$

We now consider $t_0 \to -\infty$, and we can expect that $\mathbb{G}(t, -\infty)$ vanishes because, due to coupling with the real and phantom channels, the initial state of the ring will be inconsequential at much later times. Therefore, we can write

$$\mathcal{F}(t) = \int_{-\infty}^{t} \mathbb{G}(t, t')\ \mathcal{D}(t')\ dt'. \tag{81}$$

The Green matrix can be written as

$$\mathbb{G}\left(t,t'\right)=\left(\begin{array}{cc} G^{D}\left(t,t'\right) & G^{C}\left(t,t'\right) \\ G^{*C}\left(t,t'\right) & G^{*D}\left(t,t'\right) \end{array}\right), \tag{82}$$

where each element itself is a 5×5 matrix. This allows us to write

$$\begin{aligned} f_{l}\left(t\right) &= \sum_{l'}\int_{-\infty}^{t} G_{ll'}^{D}\left(t,t'\right)\,\tilde{s}_{l'}\left(t'\right)e^{iR_{l'}t'}\,dt' \\ &+ \sum_{l'}\int_{-\infty}^{t} G_{ll'}^{C}\left(t,t'\right)\,\tilde{s}_{l'}^{\dagger}\left(t'\right)e^{-iR_{l'}t'}\,dt', \end{aligned} \tag{83}$$

and correspondingly for $f_{l}^{\dagger}(t)$. Then using the commutation relations

$$\left[\tilde{s}_{l}\left(t'\right),\tilde{s}_{l'}\left(t''\right)\right]=0, \tag{84}$$

$$\left[\tilde{s}_{l}\left(t'\right),\tilde{s}_{l'}^{\dagger}\left(t''\right)\right]=2\bar{\Gamma}_{l}\,\delta_{ll'}\,\delta\left(t'-t''\right), \tag{85}$$

it is possible to evaluate the correlation functions $\left\langle\psi_{in}\left|f_{l}\left(t\right)f_{l'}\left(t\right)\right|\psi_{in}\right\rangle$ and $\left\langle\psi_{in}\left|f_{l}^{\dagger}\left(t\right)f_{l'}\left(t\right)\right|\psi_{in}\right\rangle$, and thus $\left\langle\psi_{in}\left|\tilde{b}_{l}\left(t\right)\tilde{b}_{l'}\left(t\right)\right|\psi_{in}\right\rangle$ and $\left\langle\psi_{in}\left|\tilde{b}_{l}^{\dagger}\left(t\right)\tilde{b}_{l'}\left(t\right)\right|\psi_{in}\right\rangle$. We find

$$\begin{aligned} &\left\langle\psi_{in}\left|f_{J}\left(t_{2}\right)f_{J'}\left(t_{1}\right)\right|\psi_{in}\right\rangle \\ &=2\,\Theta\left(t_{2}-t_{1}\right)\sum_{m}\bar{\Gamma}_{m}\int_{-\infty}^{t_{1}}G_{Jm}^{D}\left(t_{2},t'\right)G_{J'm}^{C}\left(t_{1},t'\right)\,dt' \\ &+2\,\Theta\left(t_{1}-t_{2}\right)\sum_{m}\bar{\Gamma}_{m}\int_{-\infty}^{t_{2}}G_{Jm}^{D}\left(t_{2},t'\right)G_{J'm}^{C}\left(t_{1},t'\right)\,dt', \end{aligned} \tag{86}$$

and

$$\begin{aligned} &\left\langle\psi_{in}\left|f_{J}^{\dagger}\left(t_{2}\right)f_{J'}\left(t_{1}\right)\right|\psi_{in}\right\rangle \\ &=2\,\Theta\left(t_{2}-t_{1}\right)\sum_{m}\bar{\Gamma}_{m}\int_{-\infty}^{t_{1}}G_{Jm}^{*C}\left(t_{2},t'\right)G_{J'm}^{C}\left(t_{1},t'\right)\,dt' \\ &+2\,\Theta\left(t_{1}-t_{2}\right)\sum_{m}\bar{\Gamma}_{m}\int_{-\infty}^{t_{2}}G_{Jm}^{*C}\left(t_{2},t'\right)G_{J'm}^{C}\left(t_{1},t'\right)\,dt'. \end{aligned} \tag{87}$$

The reason for introducing the quantities $f_{l}(t)$ (65) is that, in the CW limit where $F_{p_1}(t)$ and $F_{p_2}(t)$ are independent of time, the coefficients of the matrix $\mathbb{M}\left(t\right)$ are also independent of time. In that limit, when $\mathbb{M}\left(t\right)=\mathbb{M}$, the elements of the full Green matrix $\mathbb{G}\left(t,t'\right)$ can be written as

$$G_{ij}\left(t,t'\right)=\sum_{k}V_{ik}\,e^{\lambda_{k}\left(t-t'\right)}\,V_{kj}^{-1}, \tag{88}$$

where the λ_{k} are the eigenvalues of $\mathbb{M}$, and the matrix element V_{ik} is the i^{th} component of the eigenvector associated with the k^{th} eigenvalue.

IX. RESULTS

In a CW experiment the squeezing spectrum can be determined by mixing the output of channel J with a bright coherent local oscillator (LO) at frequency ω_{J}, and with a tunable phase, on a 50/50 beam splitter; the outputs are then detected on two balanced fast photodiodes. The difference photocurrent from these detectors is used to capture the power spectral density of this photocurrent signal. Writing the signal and the local oscillator electric fields as

$$E\left(t\right)\propto\bar{\psi}_{J}\left(-v_{J}t,\infty\right)e^{-i\omega_{J}t}+\bar{\psi}_{J}^{\dagger}\left(-v_{J}t,\infty\right)e^{i\omega_{J}t} \tag{89}$$

and

$$E_{LO}\left(t\right)\propto\alpha\,e^{-i\omega_{J}t+i\theta}+\alpha^{*}\,e^{i\omega_{J}t-i\theta}, \tag{90}$$

where the local oscillator is considered classical with amplitude α, for a fixed θ the squeezing spectrum is given by [48, 49],

$$S\left(\Omega\right)=v_{g}\int_{-\infty}^{\infty}d\tau\,e^{-i\Omega\tau}\left\langle X_{\theta}(t)X_{\theta}(t+\tau)\right\rangle, \tag{91}$$

where

$$X_{\theta}\left(t\right)\equiv\bar{\psi}_{J}\left(-v_{J}t,\infty\right)e^{-i\theta}+\bar{\psi}_{J}^{\dagger}\left(-v_{J}t,\infty\right)e^{i\theta}. \tag{92}$$

In Appendix C we derive an analytic expression for $S\left(\Omega\right)$.

For our sample calculations we consider the ring and waveguide, each with a cross-section of $1500\,\mathrm{nm}\times800\,\mathrm{nm}$ (see Fig. 1), to be made of Si_3N_4, for which there is no two-photon absorption at telecommunication frequencies. We take the structure to be fully clad in SiO_2. The ring is assumed to have radius $R=113\,\mu m$, with loaded and intrinsic quality factors of $Q=2\times10^{5}$ and $Q_{int}=1\times10^{6}$, respectively; these factors are achievable with current technology [34, 50]. The nonlinear coefficient $\Lambda=2\pi\times0.62\,\mathrm{Hz}$ is calculated by simulating the mode profile distribution in the ring resonator using Lumerical's Mode Solutions. We initially consider CW pump fields at 1550.8 nm and 1553.6 nm, which in the "cold cavity limit" – i.e., when the microresonator is subject only to weak fields and nonlinear effects can be neglected – correspond to pump fields at ring mode orders $n_{J}=830$ (p_1) and $n_{J}=832$ (p_2); we later envision tuning to get maximum output intensity by compensating the resonances' frequencies shift due to SPM and XPM. The vacuum wavelength of resonance s in the cold cavity limit is 1551.9 nm, corresponding to ring mode order $n_{J}=831$.

Even in the cold cavity limit the frequency separations between adjacent resonances are not identical due to group-velocity dispersion. For instance, the frequency separation between the resonances s and p_2 is 3 MHz more than the separation between the resonances s and p_1. However, this is so much smaller than the average

of these two separations, which is 0.2 THz, as well as so much smaller than the optically induced shifts and the resonance linewidths discussed below, that the results we present would not be significantly modified were group-velocity dispersion neglected in the calculation.

Optically induced shifts arise as the resonances m, s, and n experience XPM from each of the pumps, while the resonances p_1 and p_2 are affected by both SPM and XPM. By "hot cavity" resonances we mean the cavity resonances in the presence of these nonlinear effects. We always consider equal pump powers in this paper, and so the frequency difference between the hot and cold cavity resonances will be $4U$ for the modes m, s, and n, and $3U$ for the modes p_1 and p_2, where $U = -\Lambda|F_{p_1}|^2 = -\Lambda|F_{p_2}|^2$ is the frequency shift of each pump resonance due to SPM. As a result, the frequency separations of the resonances in the hot resonator, as shown schematically in Fig. 3, differ from each other.

In practice, the pump detunings and the input powers are the main parameters one can adjust to optimize the squeezing achieved in the output. Although increasing the input power results in enhancing DP-SFWM, the parasitic processes SP-SFWM and BS-FWM are enhanced as well. Increasing the input power can also lead to a transition into bistable or OPO regimes [21, 51]. In this paper we avoid these regimes and only consider input powers for which the five-resonance approximation is valid, as confirmed by LLE simulations that show negligible intensity in the higher order sidebands at the pump intensities we consider.

In Fig. 4 we present the squeezing spectrum for different total input powers, where the pumps have equal powers; for each configuration the pumps are tuned to the hot cavity resonance. For the total input powers of 11, 13, 15 dBm, the hot-cavity detunings of the pumps are $-2\pi \times 49.3$, $-2\pi \times 76.3$, and $-2\pi \times 122.5$ MHz, respectively, which are small fractions of the resonance linewidth $2\bar{\Gamma}_s \approx 2\pi \times 0.97$ GHz. As can be seen, the highest degree of squeezing and anti-squeezing are achieved with the highest total input power. These calculations include the desired process, DP-SFWM, as well as all the others.

Our CMT analysis allows us to selectively turn on or off individual nonlinear processes, thus offering us an insight into their different roles. In Fig. 5 we plot the squeezing spectrum for different combinations of processes for a fixed input power, always keeping the two pumps at the hot cavity resonances and always including the DP-SFWM process.

If only the DP-SFWM process is considered, we see that we achieve higher squeezing than any other circumstance, indicating that all the additional processes considered here are parasitic. The anti-squeezing is larger than the squeezing due to the scattering loss from the ring resonator.

If only the DP-SFWM and SP-SFWM processes are considered, we find that the squeezing decreases and the anti-squeezing increases from what would result if only DP-SFWM were present. This arises because uncorrelated photons are injected into resonance s by SP-SFWM (see Fig. 2). On the other hand, if only the DP-SFWM and BS-FWM processes are considered, we find that both the squeezing and the anti-squeezing decrease from what would result if only DP-SFWM were present. This arises because photons are removed from resonance s by BS-FWM (see Fig. 2), and although the associated noise leads to a decrease in the squeezing, the removal of photons leads to a decrease in the anti-squeezing as well. Finally, we see that if we include all processes except HP-SFWM, and then compare with the situation when all processes are included, we find a small decrease in squeezing and a small increase in anti-squeezing when HP-SFWM is included. This arises because HP-SFWM injects photons in resonances m and n (see Fig. 2), which then can lead to photons being injected into resonance s through BS-FWM, analogous to the effect of SP-SFWM.

Of the parasitic processes, SP-SFWM is the most effective in reducing the squeezing, justifying efforts to design a structure to suppress this unwanted process without significantly compromising the generation efficiency [34]. Even without modifying the structure, e.g., by adding an auxiliary ring [34], and without relying on materials or designs yielding larger group velocity dispersion so that dispersion engineering can be employed [52, 53], pump detuning can be be employed as a parameter to affect the squeezing achieved in the output, and when chosen properly can lead to enhanced squeezing by suppressing the unwanted processes. To enhance the squeezing generated in the resonance s, the effectiveness of the SP-SFWM process should be degraded while keeping the DP-SFWM process as effective as possible.

This can be achieved by breaking the frequency matching condition for SP-SFWM, while keeping that for DP-SFWM. As can be seen in Figs. 2 and 3, this can be done by introducing δ_{p_1} and δ_{p_2} as detunings of the first and second pumps from the hot cavity resonances, respectively. To illustrate the effects of these pump detunings on the squeezing achieved in resonance s, in Fig. 6 we plot the squeezing in that resonance as a function of δ_{p_1} and δ_{p_2}, for a fixed total input power of 16 dBm. Focusing on SP-SFWM as the main parasitic process degrading the squeezing, we plot the generated squeezing in resonance s considering only DP-SFWM, and considering both DP-SFWM and SP-SFWM. When only DP-SFWM is considered, the highest squeezing is achieved where the two pumps tuned very close to the hot cavity resonances, $\delta_{p_1} = \delta_{p_2} = 0$; the maximum squeezing actually occurs when the detunings are negative and on the order of $2\pi \times 10$ MHz, due to both SPM/XPM effects (see Fig. 3) and group velocity dispersion. However, when SP-SFWM processes are included the highest amount of squeezing occurs far from $\delta_{p_1} = \delta_{p_2} = 0$. There are two local minima in the squeezing at points very close to the symmetric detuning line, $\delta_{p_1} = -\delta_{p_2}$. Here energy conservation still allows DP-SFWM, but forbids SP-SFWM. Yet while such a detuning configuration suppresses the

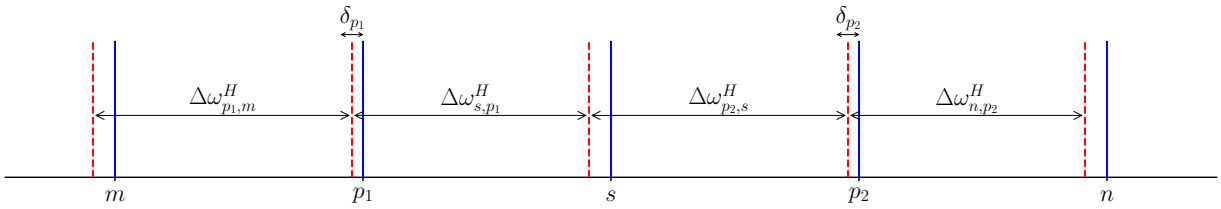


FIG. 3: (Color online) Illustration of the hot (show in red) and cold (shown in blue) cavity resonances. The resonance frequencies do not shift equally since the modes p_1 and p_2 are affected by SPM and XPM, while the modes m, s, and n are affected only by XPM. Considering the the frequency shift caused by SPM to be U, the modes p_1 and p_2 move $3U$, and the other modes move $4U$ toward lower frequencies. The detuning of the pumps from the hot-cavity resonances are indicated by δ_{p_1} and δ_{p_2}.

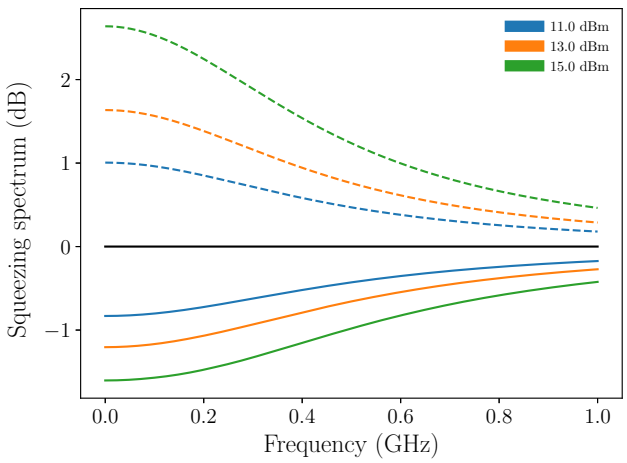


FIG. 4: (Color online) Squeezing (solid lines) and anti-squeezing (dashed lines) spectra for different input powers. The pumps are on resonance with the hot resonator. Black solid line is shot noise level.

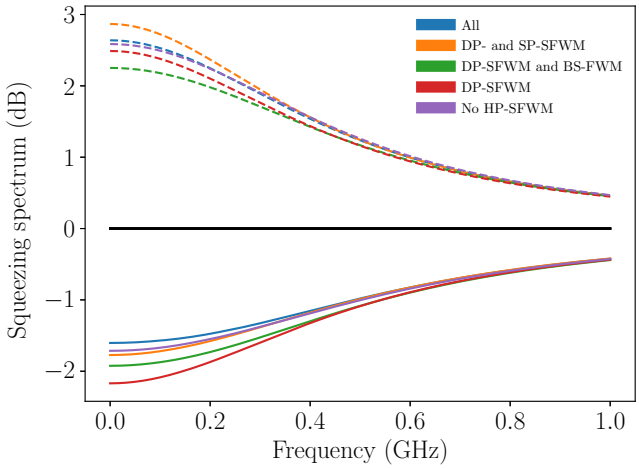


FIG. 5: (Color online) Squeezing (solid lines) and anti-squeezing (dashed lines) spectra for different combinations of nonlinear processes. Black solid line is shot noise level. The pumps are on resonance with the hot resonator. The highest squeezing is achieved when only DP-SFWM is included and the lowest is obtained when all the processes are involved.

SP-SFWM processes, it also changes the energy of the pump fields in the ring, E_{p_1} and E_{p_2} respectively for the first and second pump, and hence decreases the number of generated correlated photons in resonance s via DP-SPWM. Note that the close proximity of the two minima to the symmetric detuning line arises because of the low group velocity dispersion of the structure; this would hold generally over a few resonances for Si_3N_4 structures, but would be violated for wide frequency spans, and indeed for narrow frequency spans in structures made of other materials, such as Si.

To emphasize the role of SP-SFWM on squeezing, in Fig. 7 we plot the highest squeezing achievable by adjusting the pump detunings for a range of input powers, with and without including SP-SFWM; we also plot the anti-squeezing under these conditions. Clearly in both instances the squeezing improves as the total input power is increased. However, the parasitic effect of SP-SFWM becomes more significant at higher pump powers; as shown in the inset of Fig. 7, the difference in the maximum squeezing with and without SP-SFWM becomes more significant as the power of the pumps is increased. The result is that a higher pump power penalty is required to compensate for the parasitic effects of SP-SFWM as the level of desired squeezing is raised.

If one accepts this penalty, then significant improvements in squeezing can be achieved by detuning. Restricting our calculations to the main processes, DP-SFWM and SP-SFWM, in Fig. 8 we plot the level of squeezing that can be achieved keeping the product $E_{p_1}E_{p_2}$ fixed by adjusting the input powers, as different symmetric detunings from the hot cavity resonance – which to good approximation yield the best values of squeezing – are considered. The results presented in Fig. 8 with solid lines are obtained by setting $E_{p_1}E_{p_2} = 69.6\,\mathrm{pJ}^2$, which is the product of the energies for the total input power at 15 dBm when the pumps are

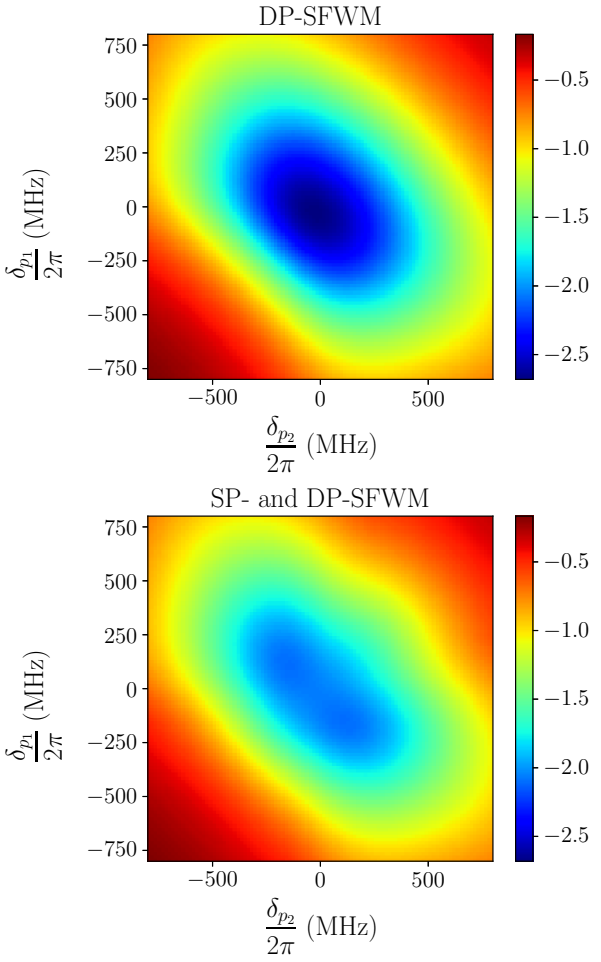


FIG. 6: (Color online) Squeezing in dB (top) when only DP-SFWM is included and (bottom) when both SP- and DP-SFWM are included as functions of the detunings of the first and the second pumps from the hot cavity resonances. Both cases have been simulated using the same total input power of 16 dBm.

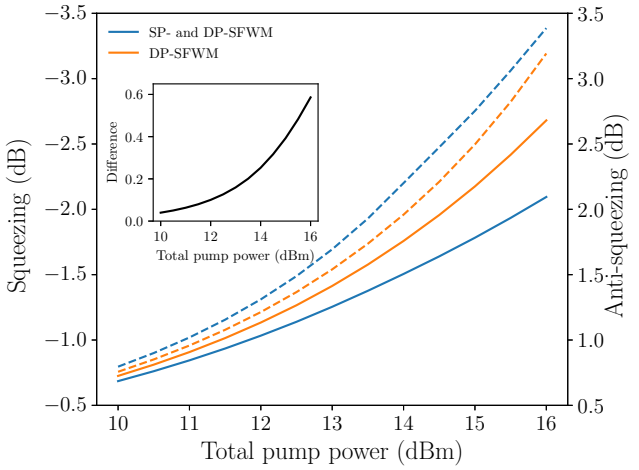


FIG. 7: (Color online) Highest squeezing (solid lines) achievable for different pump powers with and without SP-SFWM. The values have been obtained by searching for the highest values in the 2D detuning space (similar to Fig. 6) for each total input power in the range; we also plot the value of the anti-squeezing (dotted lines) under these conditions. The inset shows the difference between the highest squeezing when including SP-SFWM and the case when only DP-SFWM is considered.

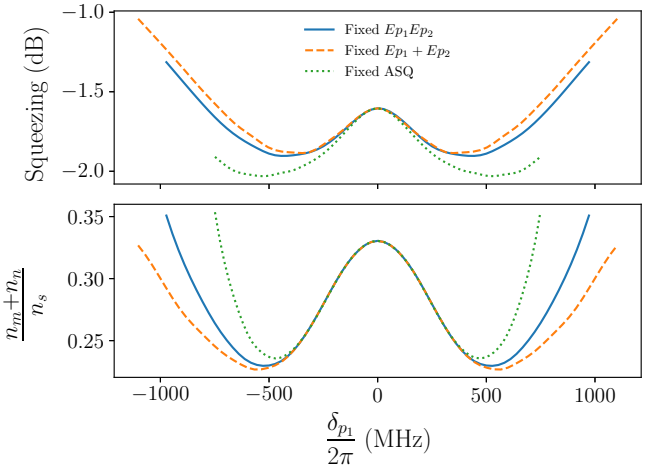


FIG. 8: (Color online) Squeezing (top) and ratio of the total generated photons in the modes m and n to the number of generated photons in the mode s (bottom) as a function of the detuning of the first pump from the hot-cavity resonance for three different scenarios of fixing the product of the energies at 69.6 pJ^2 (solid lines), total energy in the ring at 16.7 pJ (dashed lines), and anti-squeezing at 2.64 dB (dotted lines). The pumps are detuned symmetrically, i.e., $\delta_{p_1} = -\delta_{p_2}$, and the calculations included DP-SFWM and SP-SFWM.

both tuned to the hot-cavity resonances. As the product of powers is kept fixed and symmetric detuning is introduced, the total input power ranges up to 21.5 dBm over the range of detuning shown in Fig. 6. Moving away from the center ($\delta_{p_1} = 0$), there is a significant enhancement in squeezing, which is the result of suppressing the SP-SFWM while keeping the effect of DP-SFWM essentially unchanged. To confirm this, in Fig. 8 we also plot the corresponding ratio of the total number of generated photons in the modes m and n to the number of photons in the mode s. Calculating the squeezing while holding fixed the total energy in the ring, $E_{p_1} + E_{p_2}$, or the anti-squeezing in the mode s, leads to similar improvements in the squeezing, as shown in the top diagram of Fig. 8, linked to the same behavior of the photon-number ratio, as shown in the bottom of that figure.

X. CONCLUSION

We have studied the generation of squeezed vacuum states via spontaneous four-wave mixing (SFWM) in a dual-pumped nonlinear ring resonator, taking into account scattering losses in the ring and the plethora of third order nonlinear optical processes. We applied coupled-mode theory and only considered five resonances, which is a reasonable approximation for the range of input pump powers considered. This approach allowed us to investigate the role of different processes by including or omitting them in the calculation, which is not possible in calculations based on the Lugiato-Lefever equations (LLE). Including self- and cross-phase modulation allowed us to take into account hot-cavity frequency shifts. We studied CW excitation and employed a Green function strategy to calculate the relevant physical quantities, such as squeezing and the number of generated photons. We showed that parasitic processes generate uncorrelated photons in the resonance of interest, and therefore degrade the quality of squeezing in the output; the most important of these parasitic processes is single-pump SFWM. We demonstrated that without changing the ring resonator structure the use of symmetric pump detuning can suppress these unwanted processes, in particular by breaking the energy conservation condition for single-pump SFWM but not that for dual-pump SFWM. However, a power penalty must be accepted, because the dual-pump SFWM is then detuned from resonance. We intend to present LLE calculations, which are valid at higher pump powers than the five-resonance calculation used here, and studies in the regime of pulsed excitation, in future work.

Finally, it is worth mentioning that the parameters considered in this work, while achievable and indeed typical, have not been optimised to provide maximum squeezing generation efficiency. Moreover, it is possible to combine the pump-detuning technique with dispersion engineering to suppress the parasitic processes more efficiently in a dual-pumped single ring resonator configuration.

ACKNOWLEDGEMENT

This work is supported by Mitacs through the Mitacs Elevate program grant IT15614. J.E.S. acknowledges support from the Natural Sciences and Engineering Research Council of Canada (NSERC).

Appendix A

Here we reduce the expression (25) for Λ_{JKLM} in the limit where all frequencies are very close and we can take $\Lambda_{JKLM} \to \Lambda$. In this limit we use ω to denote a typical ring frequency ($\omega_J, \omega_K, \omega_L$, or ω_M), $\mathsf{d}(\boldsymbol{r}_\perp;\zeta)$ to denote a typical mode amplitude, and v to denote the group velocity of light in the ring at frequency ω. The expression (23) for $\Gamma^{ijkl}_{(3)}(\boldsymbol{r})$ neglects material dispersion, but we take the $n(\boldsymbol{r})$ there to be $n(\boldsymbol{r}_\perp;\omega)$, and use the relation

$$\mathsf{d}(\boldsymbol{r}_\perp;\zeta) = \epsilon_0 n^2(\boldsymbol{r}_\perp;\omega)\mathsf{e}(\boldsymbol{r}_\perp;\zeta), \tag{A1}$$

where $\mathsf{e}(\boldsymbol{r}_\perp;\zeta)$ is the electric field mode amplitude, to write (25) as

$$\Lambda = \frac{3\hbar\omega^2\epsilon_0}{4\mathcal{L}^2}\times \int d\boldsymbol{r}_\perp d\zeta\, \chi^{ijkl}_{(3)}(\boldsymbol{r}_\perp)\left(\mathsf{e}^i(\boldsymbol{r}_\perp;\zeta)\mathsf{e}^j(\boldsymbol{r}_\perp;\zeta)\right)^* \mathsf{e}^k(\boldsymbol{r}_\perp;\zeta)\mathsf{e}^l(\boldsymbol{r}_\perp;\zeta),$$

or

$$\Lambda = \frac{\hbar\omega v^2\gamma}{\mathcal{L}},$$

where the parameter γ is given by

$$\gamma = \frac{3\omega^2\epsilon_0}{4v^2\mathcal{L}}\times \int d\boldsymbol{r}_\perp d\zeta\, \chi^{ijkl}_{(3)}(\boldsymbol{r}_\perp)\left(\mathsf{e}^i(\boldsymbol{r}_\perp;\zeta)\mathsf{e}^j(\boldsymbol{r}_\perp;\zeta)\right)^* \mathsf{e}^k(\boldsymbol{r}_\perp;\zeta)\mathsf{e}^l(\boldsymbol{r}_\perp;\zeta).$$

Introducing typical values $\overline{\chi}_{(3)}$ and $\overline{n}$ respectively for the elements of $\chi^{ijkl}_{(3)}$ and $n(\boldsymbol{r}_\perp;\omega)$ in the region where the field amplitudes are concentrated, we can write

$$\gamma = \frac{3\omega\overline{\chi}_{(3)}}{\overline{n}^2\epsilon_0 c^2}\frac{1}{A}, \tag{A2}$$

where

$$\frac{1}{A} = \frac{\mathcal{L}^{-1}\int d\boldsymbol{r}_\perp d\zeta\, \left(\chi^{ijkl}_{(3)}(\boldsymbol{r}_\perp)/\overline{\chi}_{(3)}\right)\left(\mathsf{e}^i(\boldsymbol{r}_\perp;\zeta)\mathsf{e}^j(\boldsymbol{r}_\perp;\zeta)\right)^*\mathsf{e}^k(\boldsymbol{r}_\perp;\zeta)\mathsf{e}^l(\boldsymbol{r}_\perp;\zeta)}{\left(\int \mathsf{e}^*(\boldsymbol{r}_\perp;0)\cdot\mathsf{e}(\boldsymbol{r}_\perp;0)\frac{n(\boldsymbol{r}_\perp;\omega)/\bar{n}}{v_g(\boldsymbol{r}_\perp;\omega)/v}d\boldsymbol{r}_\perp\right)^2}, \tag{A3}$$

and we have used the normalization condition (5) together with (A1); thus (A3) can be evaluated using elec-

tric field amplitudes that are not normalized. Here A has units of area, which we see below can be identified as the effective area of the ring mode [35].

The general form of the electric field mode amplitude $\mathsf{e}(\boldsymbol{r}_\perp;\zeta)$ can be written as

$$\begin{aligned}\mathsf{e}(\boldsymbol{r}_\perp;\zeta) = &(\hat{\boldsymbol{x}}\sin\phi - \hat{\boldsymbol{y}}\cos\phi)\, e_\rho(\boldsymbol{r}_\perp)\\ &+ (\hat{\boldsymbol{x}}\cos\phi + \hat{\boldsymbol{y}}\sin\phi)\, e_\phi(\boldsymbol{r}_\perp)\\ &+ \hat{\boldsymbol{z}} e_z(\boldsymbol{r}_\perp),\end{aligned} \tag{A4}$$

where recall $\phi = \zeta/R$. It is worth considering two special cases, where the electric field is mainly in the plane of the wafer (normal to the wafer), known as TE (TM) ring modes. For a TM ring mode, to a good approximation, we can take

$$\mathsf{e}(\boldsymbol{r}_\perp;\zeta) = \hat{\boldsymbol{z}} e_z(\boldsymbol{r}_\perp). \tag{A5}$$

Then, choosing $\overline{\chi}_{(3)} = \chi_{(3)}^{zzzz}$, and using the approximation

$$\frac{n(\boldsymbol{r}_\perp;\omega)/\bar{n}}{v_g(\boldsymbol{r}_\perp;\omega)/v} \approx 1 \tag{A6}$$

in the region where the fields are concentrated, we find

$$\frac{1}{A} = \frac{\int d\boldsymbol{r}_\perp \left|e(\boldsymbol{r}_\perp)\right|^4}{\left(\int d\boldsymbol{r}_\perp \left|e(\boldsymbol{r}_\perp)\right|^2\right)^2}, \tag{A7}$$

where $e(\boldsymbol{r}_\perp) = e_z(\boldsymbol{r}_\perp)$. If instead we consider a TE ring mode, for which to good approximation we can take

$$\mathsf{e}(\boldsymbol{r}_\perp;\zeta) = (\hat{\boldsymbol{x}}\sin\phi - \hat{\boldsymbol{y}}\cos\phi)\, e_\rho(\boldsymbol{r}_\perp). \tag{A8}$$

Then assuming an isotropic material, for which $\chi_{(3)}^{xxxx} = \chi_{(3)}^{yyyy} = \chi_{(3)}^{zzzz}$ and $\chi_{(3)}^{xxyy} = \chi_{(3)}^{zzzz}/3$ (and correspondingly for all other tensor components with two x indices and two y indices), and using again the approximation (A6), we also find (A7), with now $e(\boldsymbol{r}_\perp) = e_\rho(\boldsymbol{r}_\perp)$, as might be expected. Of course, the $e_\rho(\boldsymbol{r}_\perp)$ of (A8) need not be the same as the $e_z(\boldsymbol{r}_\perp)$ of (A5).

Using (A7) in (A2) we see that since A is the effective area of the mode, within the usual approximations we have made here γ is the standard result for the waveguide nonlinear parameter of an optical fiber or channel waveguide [35]. Naturally, the expression (A3) for A can be evaluated numerically using (A4) instead of (A8) or (A5), and without the use of the approximations (A6), and the value of γ and thus of Λ determined directly. This is in fact what we do in Sec. IX.

Appendix B

Here we detail some of the steps in the derivation of (51). We first note that taking the time derivative of

$$\psi_J^o(x,t) \equiv \mathcal{U}_0^\dagger(t,0)\psi_J(x)\mathcal{U}_0(t,0), \tag{B1}$$

using (15), leads to the equation

$$\frac{\partial\psi_J^o(x,t)}{\partial t} + v_J\frac{\partial\psi_J^o(x,t)}{\partial x} = -i\omega_J\psi_J^o(x,t), \tag{B2}$$

the solutions of which are

$$\psi_J^o(x,t) = e^{-i\omega_J t}\psi_J^o(x - v_J t, 0) = e^{-i\omega_J t}\psi_J(x - v_J t). \tag{B3}$$

Thus we can write

$$\begin{aligned}&\mathcal{U}_0^\dagger(t,0)\psi_J(x)\mathcal{U}_0(t,0) = e^{-i\omega_J t}\psi_J(x - v_J t)\\ &= \int g(x,x';t)\psi_J(x')dx',\end{aligned} \tag{B4}$$

where we have defined

$$g(x,x';t) = e^{-i\omega_J t}\delta(x' - x + v_J t), \tag{B5}$$

so (B4) is the immediate generalization of (45). A corresponding result holds for the phantom channel field, and since we immediately have

$$\mathcal{U}_0^\dagger(t,0)b_J\mathcal{U}_0(t,0) = e^{-i\omega_J t}b_J, \tag{B6}$$

using the definition (35) of $V(\{\mathcal{A}_i\}\, t)$ we have, for example,

$$\mathcal{U}_0^\dagger(t,0)V\left(\{\mathcal{A}_i\};t\right)\mathcal{U}_0(t,0) = V\left(\left\{\sum_j g_{ij}(t)\mathcal{A}_j\right\}\right) \tag{B7}$$

$$\begin{aligned}&= \hbar\sum_J \gamma_J^* b_J\psi_J(-v_J t) + H.c.\\ &+ \hbar\sum_J \gamma_{Jph}^* b_J\psi_{Jph}(-v_{Jph}t) + H.c.\\ &+ H_{NL}\left(\left\{b_J e^{-i\omega_J t}\right\}, \left\{b_L^\dagger e^{i\omega_L t}\right\}\right),\end{aligned}$$

where $\psi_J(-v_J t)$, for example, is the Schrödinger operator $\psi_J(x)$ evaluated at $x = -v_J t$. We require not this but $V\left(\left\{\sum_j g_{ij}(t)\bar{\mathcal{A}}_j(t)\right\}\right)$; nonetheless, noting that (B7) can be taken to simply identify the $g_{ij}(t)$, (51) then follows.

Appendix C

Here we derive an analytic expression for $S(\Omega)$ in a case where $|\psi_{in}\rangle$ is the vacuum state; this is the situation of interest here. Using Eq. (54) in this special case we find

$$\left\langle\bar{\psi}_J^\dagger(-v_J t_2,\infty)\bar{\psi}_J(-v_J t_1,\infty)\right\rangle = \frac{\left|\gamma_J\right|^2}{v_J^2}\left\langle\tilde{b}_J^\dagger(t_2)\tilde{b}_J(t_1)\right\rangle, \tag{C1}$$

and

$$\left\langle \bar{\psi}_J(-v_J t_2,\infty)\bar{\psi}_J(-v_J t_1,\infty)\right\rangle = -\frac{\gamma_J^2}{v_J^2}\left(\left\langle \tilde{b}_J(t_2)\tilde{b}_J(t_1)\right\rangle \Theta(t_2-t_1) + \left\langle \tilde{b}_J(t_1)\tilde{b}_J(t_2)\right\rangle \Theta(t_1-t_2)\right). \quad \text{(C2)}$$

By employing Eq. (88) in Eqs. (86) and (87) we find the required expectation values in terms of the eigenvalues and eigenvectors of $\mathbb{M}(t)$ as

$$\left\langle \psi_{in}\left|\tilde{b}_J(t_2)\,\tilde{b}_J(t_1)\right|\psi_{in}\right\rangle = -2\sum_{m=1}^{N}\sum_{k'=1}^{2N}\sum_{k''=1}^{2N}\bar{\Gamma}_m\frac{V_{J\,k'}\,V^{-1}_{k'\,m}\,V_{L\,k''}\,V^{-1}_{k''\,m+N}}{\lambda_{k'}+\lambda_{k''}}\times \left(e^{\lambda_{k'}(t_2-t_1)}\Theta(t_2-t_1)+e^{\lambda_{k''}(t_1-t_2)}\Theta(t_1-t_2)\right) \quad \text{(C3)}$$

and

$$\left\langle \psi_{in}\left|\tilde{b}_J^\dagger(t_2)\,\tilde{b}_J(t_1)\right|\psi_{in}\right\rangle = -2\sum_{m=1}^{N}\sum_{k'=1}^{2N}\sum_{k''=1}^{2N}\bar{\Gamma}_m\frac{V_{J+N\,k'}\,V^{-1}_{k'\,m}\,V_{J\,k''}\,V^{-1}_{k''\,m+N}}{\lambda_{k'}+\lambda_{k''}}\times \left(e^{\lambda_{k'}(t_2-t_1)}\Theta(t_2-t_1)+e^{\lambda_{k''}(t_1-t_2)}\Theta(t_1-t_2)\right), \quad \text{(C4)}$$

where $N=5$ when only considering five modes. Letting $t_1=t_2+\tau$, and using the equations above, we can finally derive

$$S_J(\Omega) = 1-\sum_{m=1}^{N}\sum_{k'=1}^{2N}\sum_{k''=1}^{2N}\frac{\bar{\Gamma}_m}{v_g}V^{-1}_{k'\,m}\,V^{-1}_{k''\,m+N}\times \Big(e^{-2i\theta}\,\gamma_J^2\,V_{J\,k'}\,V_{J\,k''}\,A_{k',k''} - |\gamma_J|^2\,V_{J+N\,k'}\,V_{J\,k''}\,(A_{k',k''}+A_{k'',k'}) + e^{2i\theta}\,(\gamma_J^*)^2\,V_{J+N\,k'}\,V_{J+N\,k''}\,A_{k'',k'}\Big), \quad \text{(C5)}$$

where

$$A_{i,j}\equiv\frac{4\lambda_i}{(\lambda_i+\lambda_j)\,(\lambda_i^2+\Omega^2)} \quad \text{(C6)}$$

[1] C. M. Caves, Quantum-mechanical noise in an interferometer, Phys. Rev. D **23**, 1693 (1981).
[2] M. A. Taylor, J. Janousek, V. Daria, J. Knittel, B. Hage, H.-A. Bachor, and W. P. Bowen, Biological measurement beyond the quantum limit, Nature Photonics **7**, 229 (2013).
[3] N. Otterstrom, R. C. Pooser, and B. J. Lawrie, Nonlinear optical magnetometry with accessible in situ optical squeezing, Opt. Lett. **39**, 6533 (2014).
[4] E. Oelker, L. Barsotti, S. Dwyer, D. Sigg, and N. Mavalvala, Squeezed light for advanced gravitational wave detectors and beyond, Opt. Express **22**, 21106 (2014).
[5] M. I. Kolobov and C. Fabre, Quantum limits on optical resolution, Phys. Rev. Lett. **85**, 3789 (2000).
[6] N. Treps, U. Andersen, B. Buchler, P. K. Lam, A. Maître, H.-A. Bachor, and C. Fabre, Surpassing the standard quantum limit for optical imaging using nonclassical multimode light, Phys. Rev. Lett. **88**, 203601 (2002).
[7] F. Wolfgramm, A. Cerè, F. A. Beduini, A. Predojević, M. Koschorreck, and M. W. Mitchell, Squeezed-light optical magnetometry, Phys. Rev. Lett. **105**, 053601 (2010).
[8] S. L. Braunstein and H. J. Kimble, Teleportation of continuous quantum variables, Phys. Rev. Lett. **80**, 869 (1998).
[9] A. Furusawa, J. L. Sørensen, S. L. Braunstein, C. A. Fuchs, H. J. Kimble, and E. S. Polzik, Unconditional quantum teleportation, Science **282**, 706 (1998).
[10] S. Lloyd and S. L. Braunstein, Quantum computation over continuous variables, Phys. Rev. Lett. **82**, 1784 (1999).
[11] U. Andersen, G. Leuchs, and C. Silberhorn, Continuous-variable quantum information processing, Laser & Photonics Reviews **4**, 337 (2010).
[12] S. L. Braunstein and P. van Loock, Quantum information with continuous variables, Rev. Mod. Phys. **77**, 513 (2005).
[13] D. F. Walls and P. Zoller, Reduced quantum fluctuations in resonance fluorescence, Phys. Rev. Lett. **47**, 709 (1981).
[14] M. G. Raizen, L. A. Orozco, M. Xiao, T. L. Boyd, and H. J. Kimble, Squeezed-state generation by the normal modes of a coupled system, Phys. Rev. Lett. **59**, 198 (1987).
[15] Z. H. Lu, S. Bali, and J. E. Thomas, Observation of squeezing in the phase-dependent fluorescence spectra of two-level atoms, Phys. Rev. Lett. **81**, 3635 (1998).
[16] P. Grünwald and W. Vogel, Optimal squeezing in resonance fluorescence via atomic-state purification, Phys. Rev. Lett. **109**, 013601 (2012).
[17] R. E. Slusher, L. W. Hollberg, B. Yurke, J. C. Mertz, and J. F. Valley, Observation of squeezed states generated by four-wave mixing in an optical cavity, Phys. Rev. Lett. **55**, 2409 (1985).
[18] L.-A. Wu, H. J. Kimble, J. L. Hall, and H. Wu, Generation of squeezed states by parametric down conversion, Phys. Rev. Lett. **57**, 2520 (1986).
[19] Z. Vernon, N. Quesada, M. Liscidini, B. Morrison, M. Menotti, K. Tan, and J. Sipe, Scalable squeezed-light source for continuous-variable quantum sampling, Phys. Rev. Applied **12**, 064024 (2019).

[20] U. B. Hoff, B. M. Nielsen, and U. L. Andersen, Integrated source of broadband quadrature squeezed light, Opt. Express **23**, 12013 (2015).

[21] A. Dutt, K. Luke, S. Manipatruni, A. L. Gaeta, P. Nussenzveig, and M. Lipson, On-chip optical squeezing, Phys. Rev. Applied **3**, 044005 (2015).

[22] V. D. Vaidya, B. Morrison, L. G. Helt, R. Shahrokshahi, D. H. Mahler, M. J. Collins, K. Tan, J. Lavoie, A. Repingon, M. Menotti, N. Quesada, R. C. Pooser, A. E. Lita, T. Gerrits, S. W. Nam, and Z. Vernon, Broadband quadrature-squeezed vacuum and nonclassical photon number correlations from a nanophotonic device, Science Advances **6**, 10.1126/sciadv.aba9186 (2020).

[23] F. Mondain, T. Lunghi, A. Zavatta, E. Gouzien, F. Doutre, M. D. Micheli, S. Tanzilli, and V. D'Auria, Chip-based squeezing at a telecom wavelength, Photon. Res. **7**, A36 (2019).

[24] S. Clemmen, K. P. Huy, W. Bogaerts, R. G. Baets, P. Emplit, and S. Massar, Continuous wave photon pair generation in silicon-on-insulator waveguides and ring resonators, Opt. Express **17**, 16558 (2009).

[25] W. Bogaerts, P. De Heyn, T. Van Vaerenbergh, K. De Vos, S. Kumar Selvaraja, T. Claes, P. Dumon, P. Bienstman, D. Van Thourhout, and R. Baets, Silicon microring resonators, Laser & Photonics Reviews **6**, 47 (2012).

[26] Z. Vernon and J. E. Sipe, Spontaneous four-wave mixing in lossy microring resonators, Phys. Rev. A **91**, 053802 (2015).

[27] P. Del'Haye, A. Schliesser, O. Arcizet, T. Wilken, R. Holzwarth, and T. J. Kippenberg, Optical frequency comb generation from a monolithic microresonator, Nature **450**, 1214 (2007).

[28] G. Lin, A. Coillet, and Y. K. Chembo, Nonlinear photonics with high-q whispering-gallery-mode resonators, Adv. Opt. Photon. **9**, 828 (2017).

[29] M. Ferrera, L. Razzari, D. Duchesne, R. Morandotti, Z. Yang, M. Liscidini, J. E. Sipe, S. Chu, B. E. Little, and D. J. Moss, Low-power continuous-wave nonlinear optics in doped silica glass integrated waveguide structures, Nature Photonics **2**, 737 (2008).

[30] A. Melloni, F. Morichetti, and M. Martinelli, Linear and nonlinear pulse propagation in coupled resonator slow-wave optical structures, Optical and Quantum Electronics **35**, 365 (2003).

[31] H. Seifoory, L. G. Helt, J. E. Sipe, and M. M. Dignam, Counterpropagating continuous-variable entangled states in lossy coupled-cavity optical waveguides, Phys. Rev. A **100**, 033839 (2019).

[32] M. Kamandar Dezfouli and M. M. Dignam, Photon-pair generation in lossy coupled-resonator optical waveguides via spontaneous four-wave mixing, Phys. Rev. A **95**, 033815 (2017).

[33] H. Seifoory and M. M. Dignam, Squeezed-state evolution and entanglement in lossy coupled-resonator optical waveguides, Phys. Rev. A **97**, 023840 (2018).

[34] Y. Zhang, M. Menotti, K. Tan, V. D. Vaidya, D. H. Mahler, L. G. Helt, L. Zatti, M. Liscidini, B. Morrison, and Z. Vernon, Squeezed light from a nanophotonic molecule, Nature Communications **12**, 2233 (2021).

[35] R. Boyd, *Nonlinear Optics* (Elsevier Science, 2019).

[36] L. G. Helt, A. M. Brańczyk, M. Liscidini, and M. J. Steel, Parasitic photon-pair suppression via photonic stop-band engineering, Phys. Rev. Lett. **118**, 073603 (2017).

[37] Y. Zhao, Y. Okawachi, J. K. Jang, X. Ji, M. Lipson, and A. L. Gaeta, Near-degenerate quadrature-squeezed vacuum generation on a silicon-nitride chip, Phys. Rev. Lett. **124**, 193601 (2020).

[38] S. Ramelow, A. Farsi, Z. Vernon, S. Clemmen, X. Ji, J. E. Sipe, M. Liscidini, M. Lipson, and A. L. Gaeta, Strong nonlinear coupling in a si_3n_4 ring resonator, Phys. Rev. Lett. **122**, 153906 (2019).

[39] N. A. R. Bhat and J. E. Sipe, Hamiltonian treatment of the electromagnetic field in dispersive and absorptive structured media, Phys. Rev. A **73**, 063808 (2006).

[40] J. E. Sipe, Photons in dispersive dielectrics, Journal of Optics A: Pure and Applied Optics **11**, 114006 (2009).

[41] J. E. Sipe and M. J. Steel, A hamiltonian treatment of stimulated brillouin scattering in nanoscale integrated waveguides, New Journal of Physics **18**, 045004 (2016).

[42] M. Jasperse, L. D. Turner, and R. E. Scholten, Relative intensity squeezing by four-wave mixing with loss: an analytic model and experimental diagnostic, Opt. Express **19**, 3765 (2011).

[43] H. Seifoory, S. Doutre, M. M. Dignam, and J. E. Sipe, Squeezed thermal states: the result of parametric down conversion in lossy cavities, J. Opt. Soc. Am. B **34**, 1587 (2017).

[44] A. E. Ulanov, I. A. Fedorov, A. A. Pushkina, Y. V. Kurochkin, T. C. Ralph, and A. I. Lvovsky, Undoing the effect of loss on quantum entanglement, Nature Photonics **9**, 764 (2015).

[45] J. E. Sipe, N. A. R. Bhat, P. Chak, and S. Pereira, Effective field theory for the nonlinear optical properties of photonic crystals, Phys. Rev. E **69**, 016604 (2004).

[46] S. N. Volkov and J. E. Sipe, Nonlinear optical interactions of wave packets in photonic crystals: Hamiltonian dynamics of effective fields, Phys. Rev. E **70**, 066621 (2004).

[47] Z. Vernon, *Microresonators for Nonlinear Quantum Optics*, Ph.D. thesis (2017).

[48] A. A. Clerk, M. H. Devoret, S. M. Girvin, F. Marquardt, and R. J. Schoelkopf, Introduction to quantum noise, measurement, and amplification, Rev. Mod. Phys. **82**, 1155 (2010).

[49] J. Cresser, Theory of the spectrum of the quantised light field, Physics Reports **94**, 47 (1983).

[50] J. M. Arrazola, V. Bergholm, K. Brádler, T. R. Bromley, M. J. Collins, I. Dhand, A. Fumagalli, T. Gerrits, A. Goussev, L. G. Helt, J. Hundal, T. Isacsson, R. B. Israel, J. Izaac, S. Jahangiri, R. Janik, N. Killoran, S. P. Kumar, J. Lavoie, A. E. Lita, D. H. Mahler, M. Menotti, B. Morrison, S. W. Nam, L. Neuhaus, H. Y. Qi, N. Quesada, A. Repingon, K. K. Sabapathy, M. Schuld, D. Su, J. Swinarton, A. Száva, K. Tan, P. Tan, V. D. Vaidya, Z. Vernon, Z. Zabaneh, and Y. Zhang, Quantum circuits with many photons on a programmable nanophotonic chip, Nature **591**, 54 (2021).

[51] I. D. Rukhlenko, M. Premaratne, and G. P. Agrawal, Analytical study of optical bistability in silicon ring resonators, Opt. Lett. **35**, 55 (2010).

[52] T. J. Kippenberg, A. L. Gaeta, M. Lipson, and M. L. Gorodetsky, Dissipative kerr solitons in optical microresonators, Science **361**, 10.1126/science.aan8083 (2018).

[53] S. Kim, K. Han, C. Wang, J. A. Jaramillo-Villegas, X. Xue, C. Bao, Y. Xuan, D. E. Leaird, A. M. Weiner, and M. Qi, Dispersion engineering and frequency comb generation in thin silicon nitride concentric microres-

onators, Nature Communications **8**, 372 (2017).